Constraint-Aware Model Predictive Control of Fuel Cell Oxygen Excess Ratio and Cathode Pressure to Maximize Power Output

Ankit Kulkarni, Nicolai Waycaster, Rishie Aravind Madhu, Rohit Ravikumar, Sai Vithal Pennumacha
Clemson University

Abstract

Due to the current challenges posed by global warming and the limited supply of traditional fuel sources, there is a growing necessity to transition to alternative power generation methods for vehicles. Fuel cells, known for clean operation, high power density, quiet operation, and efficiency, hold significant promise in replacing conventional energy sources. To optimize the potential of fuel cells, accurate control of the airpath is crucial. This project's objective is to apply model predictive control (MPC) controller to the airpath dynamics to track oxygen excess ratio (OER) and cathode pressure, ensuring the safe operation of the fuel cell and maximizing its power output. A non-linear plant model has been developed for the fuel cell airpath. This non-linear plant is linearized across single as well as 1000 nominal points, the advantages of using 1000 nominal points have been discussed. A setpoint tracking model predictive controller is devised to generate control inputs for the plant such that the setpoints are tracked to certain value. It was observed that the maximum power that could be generated was 69.66 kW.

Introduction

The control of a PEMFC airpath system was proposed previously in phase 1. The main parameters of importance in the airpath were oxygen excess ratio (OER) and cathode pressure. OER is the ratio between the inlet oxygen mass flow and reacted oxygen mass flow. OER has a large impact on the power generated by the stack and the safe operation of the fuel cell. It is highly important to maintain OER within a set value to prevent damage and minimize voltage drop [1]. Cathode pressure influences the dynamic response of the fuel stack to load current draw and the output power [2]. Therefore, it is very important to track both OER and Cathode pressure together to achieve the objective of fuel cell airpath control as both are interdependent and crucial to the power output of the fuel cell.

Dynamic Airpath Plant Model

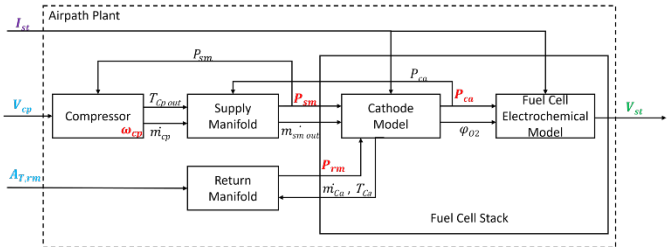

Figure 1. Fuel Cell Airpath Plant Model

A fuel cell airpath plant model has been developed as shown in fig.1. The plant consists of mainly five elements: the compressor which ensures sufficient oxygen flow and replenishment, the supply and return manifolds which are a lump of all pipes, the cathode model which calculates the cathode pressure ($\boldsymbol{P_{ca}}$) and the oxygen excess ratio ($\boldsymbol{\varphi_{O2}}$), and the electrochemical model which calculates the terminal voltage of the fuel cell stack. These are governed by the following differential equations [3][4][5][6]:

$$\frac{d\omega_{cp}}{dt} = \frac{\tau_{cm} - \tau_{cp}}{J_{cp}} \tag{1}$$

$$\frac{dP_{sm}}{dt} = \frac{R_A T_{cp}}{V_{sm}}\left(\dot{m}_{cp} - \dot{m}_{sm\,out}\right) \tag{2}$$

$$\frac{dP_{ca}}{dt} = \left(\frac{R_A T_{st}\,\dot{m}_{ca\,in}}{V_{ca}} - \frac{R_A T_{st}\,\dot{m}_{ca\,out}}{V_{ca}} - K_{CaCur} I_{st}\right) \tag{3}$$

$$\frac{dP_{rm}}{dt} = \frac{R_A T_{rm}}{V_{rm}}\left(\dot{m}_{ca\,out} - \dot{m}_{rm\,out}\right) \tag{4}$$

$$\varphi_{O2} = \frac{Inlet\ oxygen\ mass\ flow}{Reacted\ oxygen\ mass\ flow} = \frac{\dot{m}_{O2\,ca\,in}}{\dot{m}_{O2\,rct}} \tag{5}$$

$$V_{st} = N_{st} * \left[E_{nerst} - V_{ohm} - V_{concentration}(P_{ca}) - V_{act}(\varphi_{O2})\right] \tag{6}$$

Based on the above governing equations, a four-state non-linear dynamic plant model is built in Simulink with compressor speed ($\boldsymbol{\omega_{cp}}$), supply manifold pressure ($\boldsymbol{P_{sm}}$), cathode pressure ($\boldsymbol{P_{ca}}$), and return manifold pressure ($\boldsymbol{P_{rm}}$) as the states with control inputs as the compressor voltage ($\boldsymbol{V_{cp}}$) and throttle valve opening area ($\boldsymbol{A_{T,rm}}$) along with the stack current ($\boldsymbol{I_{st}}$) modeled as a disturbance. The tracking variables are, OER ($\boldsymbol{\varphi_{O2}}$), and Cathode Pressure ($\boldsymbol{P_{ca}}$). The plant outputs are the system states, stack voltage ($\boldsymbol{V_{st}}$), ($\boldsymbol{\varphi_{O2}}$), Power output of the fuel cell stack ($\boldsymbol{p_{fS}}$), and compressor mass flow rate ($\boldsymbol{\dot{m}_{Cp}}$)

$$x = [\omega_{cp} \quad P_{sm} \quad P_{rm} \quad P_{ca}\ ]^T \tag{7}$$

$$u = [A_{T,rm} \quad V_{cp}]^T \tag{8}$$

$$d = I_{st} \tag{9}$$

$$\dot{x} = f(x, u, d) \tag{10}$$

$$z = [\varphi_{O2} \ P_{ca}\ ]^T \tag{11}$$

$$y = [x \ V_{st} \ \varphi_{O2} \ p_{fS} \ \dot{m}_{Cp}]^T \tag{12}$$

Drive Cycle Data

Drive cycle data of stack current was acquired from the benchmark paper [3]. Stack current is taken as a disturbance to the Simulink model. To validate the Simulink model under open loop conditions, control inputs had to be generated for sanity checks of the plant. The compressor voltage was taken from the results obtained in [3]. The Throttle input was taken as a step change from 0 to 50 percent. A lookup table was constructed to represent the compressor map data

which was obtained from [3]. Fig.2 shows the compressor voltage and disturbance which were used for open loop plant simulation.

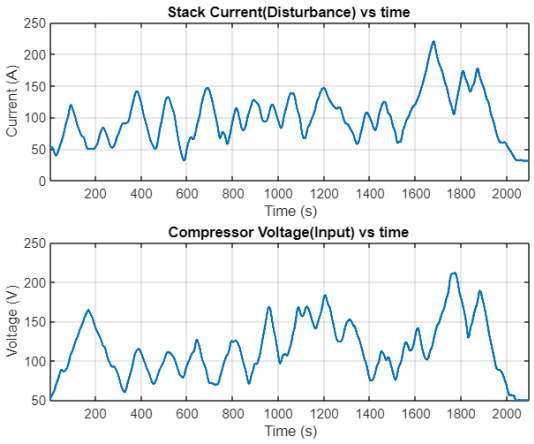

Figure 2. Open Loop Inputs

Open Loop Simulation Results

The tracking parameters of OER and Cathode pressure were plotted and compared to the benchmark paper [3]. Fig. 3 shows the variations of tracking variables under open-loop inputs. The maximum OER is around 6. From the literature review conducted in phase 1, it was pointed out that such values of OER will lead to a drop in power output of fuel cell. This happens because the compressor actuation must be increased to supply higher levels of oxygen leading to increased parasitic loss and reducing system power. Moreover, OER below 1.5 leads to oxygen starvation and can severly damage the stack. This shows that it is critical to control OER to maximize the power output and also ensure it does not fall below 1.5 resulting in possible damage the cell stack [4]. In Fig. 3, the cathode pressure varies from 1 bar to 1.5 bar. Literature survey suggests that the optimal value of Cathode pressure should be between 1 and 1.5 bar to obtain the best perfomance of the fuel cell [6].

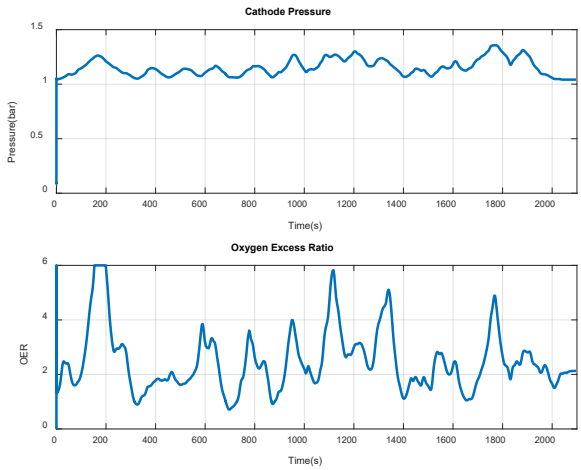

Figure 3. Open Loop Results

The output voltage of the fuel cell is plotted for the given drive cycle. The trend of the output was similar to the results of the benchmark paper [3] which validated the non-linear plant model.

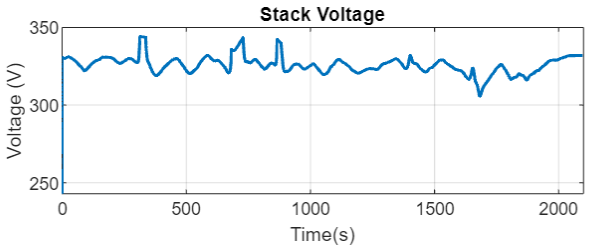

Figure 4. Open Loop Output Voltage

Fig. 4 and 5 shows the system state trajectories for open loop simulation. The compressor speed reaches a maximum speed of 130 kRPM which is greater than the physical limitations of the compressor. This calls for control on compressor speed using compressor motor voltage control. The supply manifold pressure reaches a maximum of 1.5 bar and the return manifold pressure varies little. It was observed that the plant has different sensitivities towards different control inputs and the change in tracking variables affects the final output of the plant. As a result, sensitivity analysis was conducted and discussed in the next section.

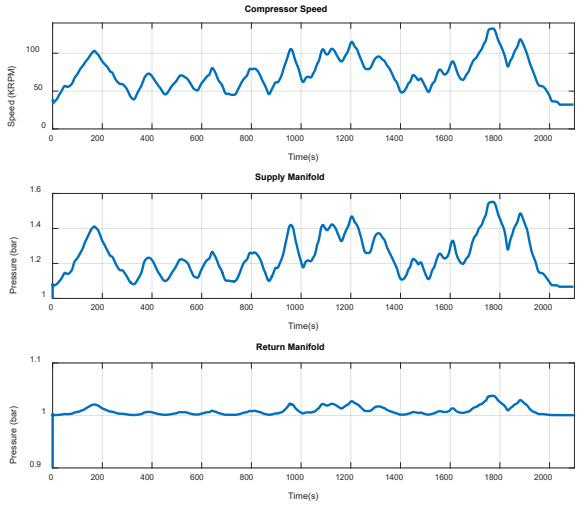

Figure 5. Open Loop States

Sensitivity Analysis

Sensitivity analysis was conducted on the airpath model using the Sensitivity Analyzer app from the Simulink Design Optimization Toolbox. The sensitivity of the tracking variables over the full actuation range of the control variables needed to be determined [7]. Fig. 6 below shows the results of this analysis. Values for specific parameter sensitivity were also given by the app. The values are given on a scale from zero to one. A value closer to one indicates high sensitivity in relation to a specific parameter while a value closer to zero indicates low sensitivity. The sign of the value indicates a negative or positive correlation. OER had a sensitivity of 0.1981 to throttle area and 0.9027 to compressor voltage. Cathode pressure had a sensitivity of -0.2986 to throttle area and 0.6478 to compressor voltage. Both tracking variables had higher sensitivity to compressor voltage than throttle area. As such, precise and responsive control of compressor voltage over throttle area was prioritized for best controller performance.

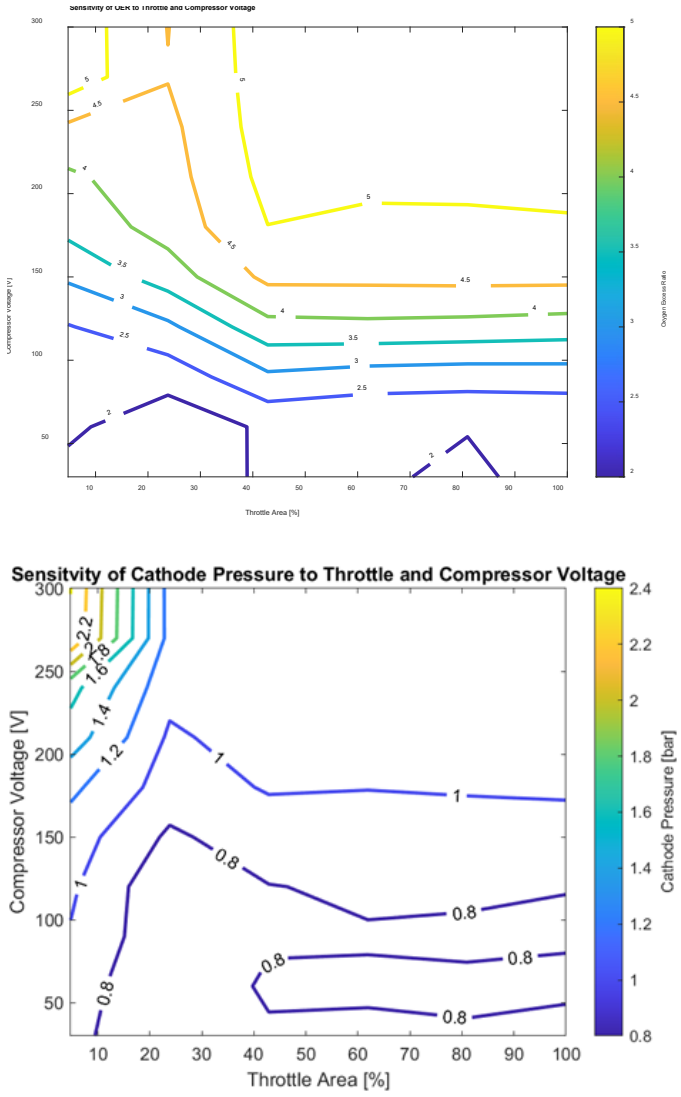

Figure 6. Tracking Variable Sensitivity Contours

The second set of sensitivity analyses shown in Fig. 7 tested the sensitivity of the performance variable (mean power output over the drive cycle) over the tracking variable ranges determined in the first test (see the color bars in Fig. 6) and control variable actuation ranges. Fig. 7 shows the results of this analysis. Power output had a sensitivity value of -0.0835 to OER, 0.9016 to cathode pressure, 0.1171 to throttle area, and 0.3229 to compressor voltage.

These results show the plant has greater sensitivity to compressor voltage than throttle area on the control input side. As OER begins to rise above 4, the power starts to drop due to increased parasitic losses. However, across the drive cycle tested, OER has very little impact on performance compared to cathode pressure. Moreover, the model performance is more sensitive towards cathode pressure, changing the power output significantly. This makes tracking cathode pressure significantly more important than OER. These learnings were used to develop the control strategy to be most efficient. During MPC tuning, more weight was given to cathode pressure setpoint tracking rather than OER.

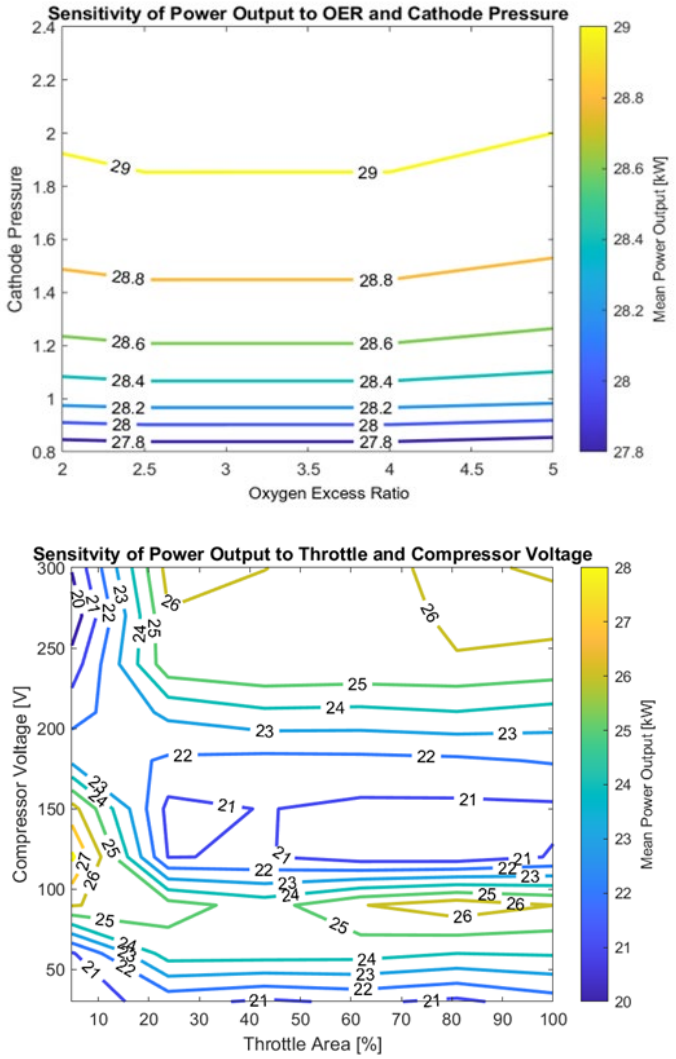

Figure 7. Output Sensitivity Contours

Linearization

To implement an MPC the plant model first required linearization, for which multiple approaches have been discussed in this section.

Single nominal point linearization

Initially, the plant model was linearized using a single nominal point for both the control inputs $[\boldsymbol{A_{T,rm}} \quad \boldsymbol{V_{cp}}]^{\boldsymbol{T}}$ and the disturbance I_{st} as the inputs for the plant and V_{st} as the output. This plant model was run for 100 seconds with model inputs set to nominal points and MATLAB's *linmod* function was used to linearize the plant with the output of the simulation. The average of the minimum and maximum points of each input found in the benchmark data were taken as the nominal points for the single point linearization. The drive cycle discussed earlier was used for state tracking and output tracking with a single nominal point. The output of the *linmod* function are state space matrices which can be represented in the equations shown below.

$$\dot{\delta x} = A\delta x + B\delta u \quad \& \quad \delta y = C\delta x + D\delta u \qquad (13,14)$$

$$\delta u = u - u_e, \;\; x = \delta x + x_e \;\; \& \;\; y = \delta y + y_e \qquad (15, 16, 17)$$

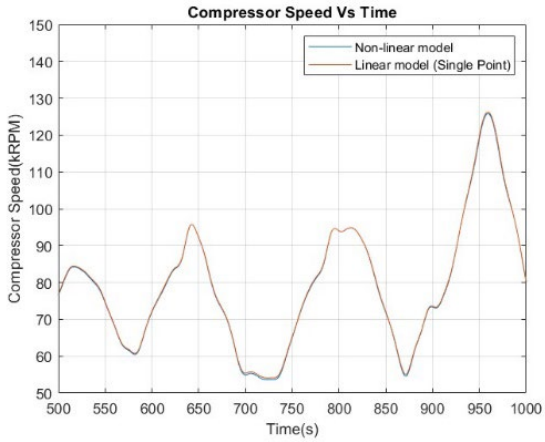

Figure 8. Compressor Speed Tracking

The state tracking using the single nominal point was acceptable as shown in Fig. 8. However, to improve the tracking, a new approach was introduced which will be discussed later. All eigen values of this continuous state space system were shown to have negative real values shown below. Thus, the continuous system was found to be stable.

$$eig(A) = [-1.9e+05;\ -2.7e+04;\ -4.45;\ -381.79] \quad (18)$$

Also, the time constant calculation was done to understand the sample time requirement for implementing the MPC. The formula used for calculation of the time constant is provided below.

$$\Delta t = \frac{1}{|eig(A)|} = 0.225\ s \quad (19)$$

Considering the calculated time constant, sampling time of 0.1 seconds (10ms) was chosen for best MPC performance.

Multiple nominal point linearization

The single nominal point linearized model works only within a certain range of inputs close to the nominal points used for linearization. Understanding the behavior of the plant model and identifying the points where this model does not hold well is a very time-consuming process especially for a system with multiple inputs. Non-linear MPC (NMPC) was also considered as a controller for the system, however, due to the immense computation power and time required, it was not considered as a final option for controller. A novel approach was introduced to counter these issues by introducing multiple pre-calculated linearized systems for MPC. Ten equally spaced nominal points were considered for each input to the plant model. Considering all the combinations, the plant model was linearized for 1000 unique nominal points and the output of the linearization (i.e., the state space matrices and the nominal output points) were stored in 10x10x10 3D cell arrays. These arrays can be easily accessed similarly to a lookup table for MPC calculations. This saves a significant amount of computation while running an MPC reducing the sample rate at which the MPC can be run and produces better tracking of setpoints. Furthermore, this can potentially remove the necessity of using an NMPC which requires much more computation time and power. Table 1 documents the deviation of state tracking by the single point model and the 1000-points model with respect to the non-linear model.

Table 1. Comparison between Single Point and 1000-points model

Deviation with respect to the Non-linear model		States			
		ω_cp	P_sm	P_rm	P_ca
Single Point	Avg. Error (%)	3.414	1.225	0.462	0.958
	Max. Error (%)	107.732	47.155	179.654	74.412
1000 Points	Avg. Error (%)	1.762	0.588	0.049	0.409
	Max. Error (%)	16.179	2.747	0.285	1.842

A consistent improvement of average deviation is observed in the 1000-points model for all the states. Crucially, the 1000-points model reduces the maximum deviations observed during the state tracking significantly. Fig. 9 shows a comparison between the single point model and the 1000-points model for return manifold pressure.

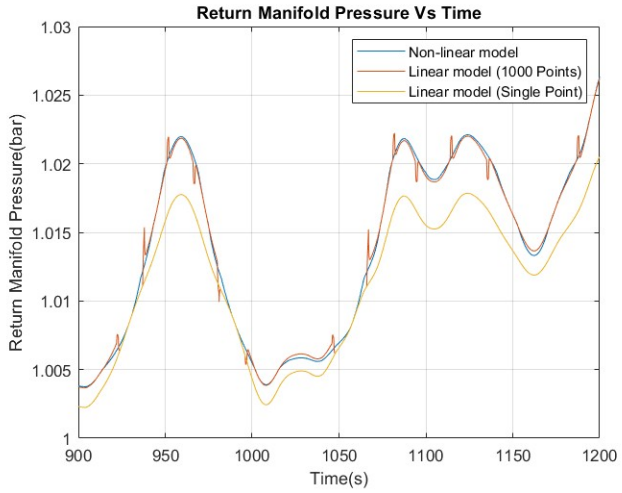

Figure 9. Return Manifold Pressure Tracking

As seen in Fig. 9, the state tracking for return manifold pressure with single point model was already very good. The significant improvement of tracking using the 1000-points method showcases the effectiveness of the approach. The kinks observed in the state tracking using 1000-point method signify the points where a considerable change in the input conditions causes a change in the linear model being used. At certain regions in Fig. 9, it can be observed that both the tracking plots merge as the nominal points coincide during that part of the drive cycle.

Control Strategy

The main objective of the MPC controller is to minimize the tracking error between the setpoints and the model output of the measured parameters of OER and P_{ca} . Thus, a tracking MPC has been employed. The setpoints for these parameters are originally generated through a set point optimizer in the benchmark paper. [3] Since the aim of this project is to design and test the lower-level controller, the set point data from [3] was used as a lookup table (Fig.10). These setpoints are chosen such that they result in maximized power output. This reduces the main goal of the MPC to just ensure optimum setpoint tracking.

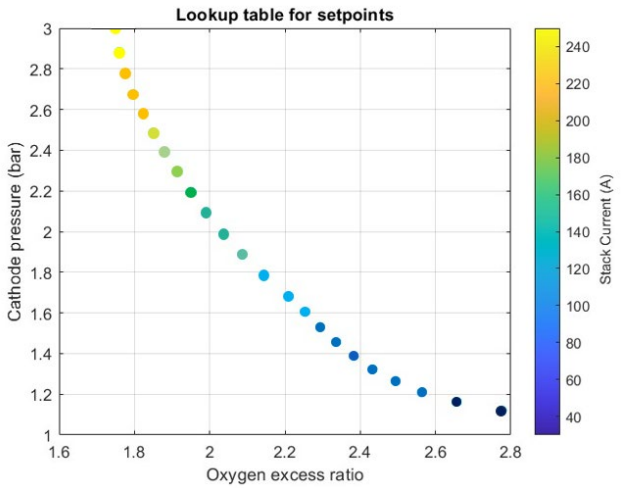

Figure 10. Set Point Lookup Table

Cost function

$$\min J = \sum_{k=1}^{N-1}\left(z_k - z_k^{sp}\right)^T Q\left(z_k - z_k^{sp}\right) + \sum_{k=1}^{M-1}(u_k - u_{k-1})^T R(u_k - u_{k-1}) \quad (20)$$

$$s.t. \quad \delta x_{k+1} = A_d \delta x_k + B_d \delta u_k$$

$$0 \leq u(At) \leq 0.022\ [in\ m],$$

$$0 \leq u(v_{Cm}) \leq 350\ [in\ V]$$

$$1.5 \leq \varphi_{O2} \leq 4$$

The MPC aims to track these setpoints which will ensure that the power output of the fuel cell is maximized. The cost function also has a rate-limiting term for both the throttle and compressor voltage inputs to penalize rapid change in control inputs. This accounts for the physical limitations of the actuators. The cost function is subjected to the state equation and actuator limits. The solver used for optimization is *fmincon* function which by default uses the interior point method.

MPC Formulation

The preview horizon (N) is 10 steps, and the sampling time (dt) is 0.1s. Initially N was taken as 40, but soon reduced to 10 to improve the computation time and the length of the drive cycle. It was found that the performance change from 40 to 10 was not drastic and therefore the value was fixed. The optimizing variable is u (A_t, V_{cp}), which has the two inputs augmented over the horizon to form a (N*(n+m),1) array. As the stack current is a disturbance to the system, the B matrix that is obtained after discretization is split into B and B_w matrices to make it more convenient. In the MPC formulation, the entire preview horizon of the disturbance was used to better help the MPC to track for upcoming known disturbances (i.e., the current values over the horizon steps). The cost function was called inside the *fmincon* solver which calculated the total cost over the horizon for a particular time step. The MPC uses a discretized plant model as a step time to calculate the states with the optimal input sequence as generated by the solver. The initial states (x_0) are taken as the nominal points, and the plant progresses from there.

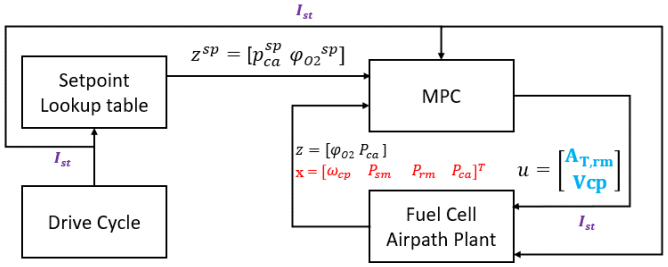

Figure 11. Control System Architecture

Fig. 11 shows the implementation of the controller on the plant. The controller takes setpoints for the tracking variables, disturbance, and the plant outputs as inputs and computes the optimal control inputs to be given to the plant to realize the tracking objective and enforce the constraints.

Tuning

The main tuning parameters that directly affect the tracking performance and the computation time are the prediction horizon, control horizon, the weights assigned to each tracking parameter and input rate of change. The tuning parameters selection is a laborious process that involves a lot of tuning effort and therefore a systematic process was adopted here which considered root mean square error, simulation time, maximum power output, and mean power output. In this project, two parameters were to be tracked, oxygen excess ratio (φ_{O2}) and cathode pressure (P_{ca}). Based on tests, changing the weightage of one greatly affected the tracking of the other parameter, requiring a tradeoff to be made. Table 2 shows this conclusion. The R value selected was conservative at first to reduce the actuation rates, but this led to a reduced tracking performance. Hence a more aggressive actuation strategy was used, and a lower value R value was chosen.

Table 2. Control Calibration Results

Iteration Number	Diag (Q)	Diag (R)	Peak Power [kW]	Root Mean Square Error	
				P_{ca} [bar]	OER
1	[3200,80]	[1,800]	67.10	0.1016	0.6208
2	[32e3,800]	[1,0]	61.81	0.2840	0.2076
3	[39e2,600]	[1,0]	70.31	0.1043	0.3316
4	[390,60]	[1,0]	51.81	0.3368	0.2161
5	[39e3,600]	[1,0]	69.66	0.0335	0.2388
6	[39e3,600]	[1,1]	64.57	0.0787	0.2237

Results

From Table 2, iteration number 5 was selected as the final tuned parameters as they resulted in the highest average as well as peak power outputs among all iterations. The system was simulated with the tuned MPC parameters of iteration 5. Fig.12 shows the state trajectories. The maximum compressor speed peaks at around 110 kRPM which is within the operating region of the selected compressor from the benchmark paper. The return manifold pressure is the least of the three followed by cathode pressure and the supply manifold pressure is the maximum, which is in line with the expected trend. Fig.13 captures the output trajectories. The stack voltage reaches values of 330V which leads to peak power output of 69.66 kW. The average power output over the drive cycle is 31.83 kW. The compressor mass flow rate reaches a peak of 0.09 kg/s which is within the physical limits of the compressor.

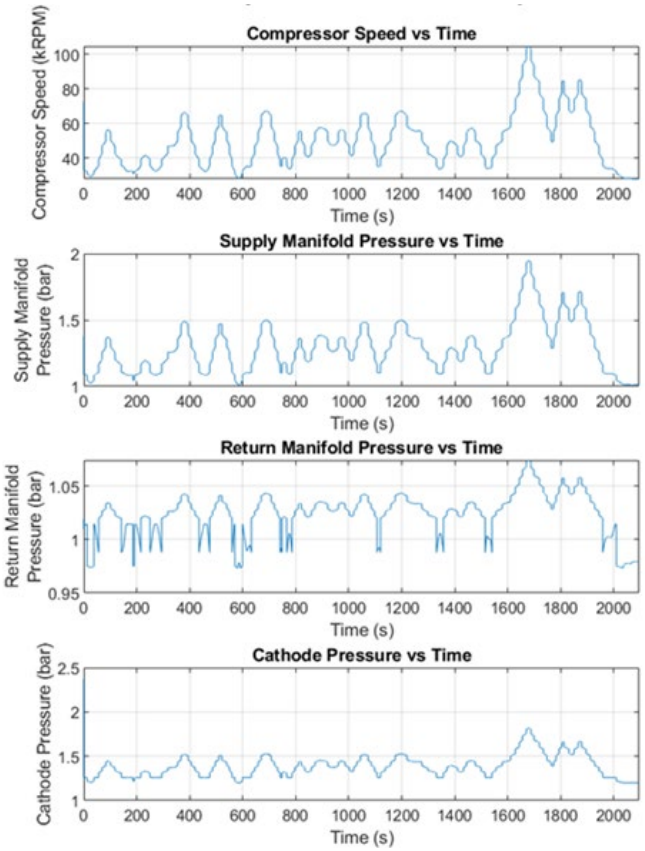

Figure 12. State Trajectory Plots

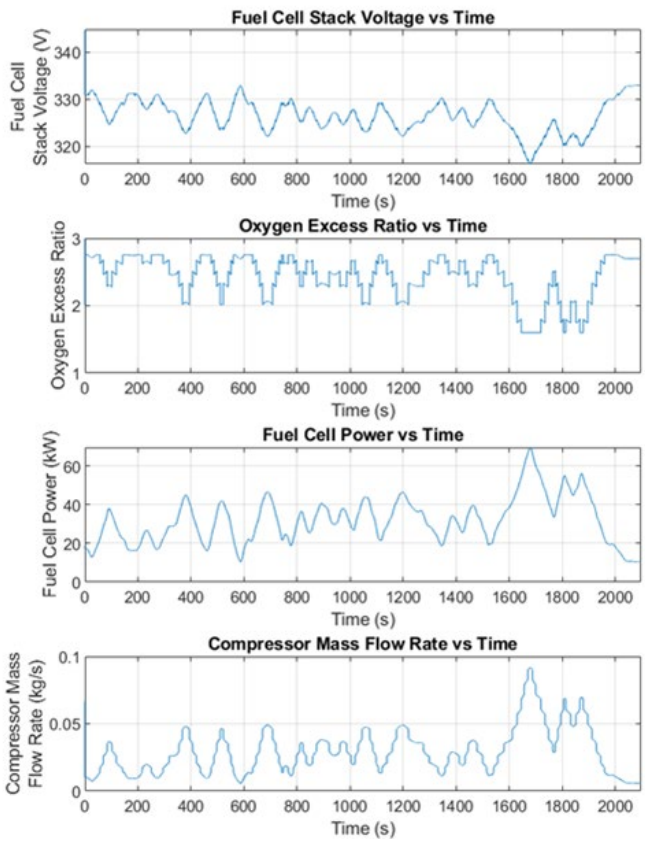

Figure 13. Output Trajectory Plots

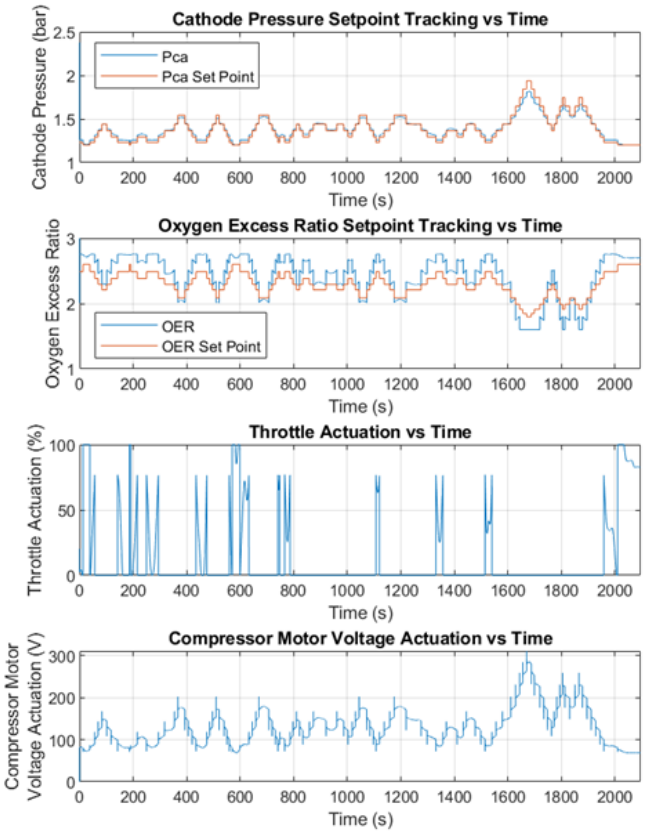

Figure 14. Set Point Tracking and Actuator Trajectories over Drive Cycle

From Fig.14 it is clear that P_{ca} tracked nearly perfectly. Since (P_{ca}) and (φ_{O2}) are closely coupled, it is not possible to track both the parameters to match the set points throughout the drive cycle. Increasing φ_{O2} will increase (P_{ca}) and vice versa, which means a tradeoff needs to be made in terms of the tracking variables. Since the sensitivity analysis results shown in Fig. 7 proved that (P_{ca}) has more impact on the output of the fuel cell, more weightage was given to the tracking of (P_{ca}). However, the objective of maintaining (φ_{O2}) below 4 to avoid the power drop and ensuring that it does not fall below 1.5 to prevent damage to the cell stack has been achieved.

Conclusion

A non-linear fuel cell model was built and validated. The model was linearized around 1000 nominal points to effectively capture the dynamics. A tracking MPC controller was designed to track oxygen excess ratio and cathode pressure by optimizing the control inputs of the fuel cell plant. The designed controller was able to track the setpoints decently well with a tradeoff adopted to give more weightage to Cathode pressure tracking and maintain OER within a set bound. The results obtained prove that the MPC controller maximized the power output and ensured the safe operation of the fuel cell.

Future Scope

As a continuation to this project, temperature dynamics and effects of membrane hydration can be added to the plant model which would improve the accuracy of the same. Also, a deep learning algorithm can be used to predict driver behavior and throttle actuations which can be fed into the MPC as the preview horizon.

Appendix

Model Equations

1. Compressor Model

$$\tau_{cm} = \eta_{cm} \frac{k_t}{R_{cm}} (V_{cp} - k_v \omega_{cp}) \quad (21)$$

$$\tau_{cp} = \frac{C_p T_{atm}}{\omega_{cp} \eta_{cp}} \left(\left(\frac{P_{sm}}{P_{atm}} \right)^{\frac{\gamma-1}{\gamma}} - 1 \right) \dot{m}_{cp} \quad (22)$$

$$T_{cp\,out} = \frac{T_{atm}}{\eta_{cp}} \left(\eta_{cp} + \left(\frac{P_{sm}}{P_{atm}} \right)^{\frac{\gamma-1}{\gamma}} - 1 \right) \quad (23)$$

2. Supply Manifold Model

$$\dot{m}_{sm\,out} = K_{sm}(P_{sm} - P_{ca}) \quad (24)$$

3. Cathode Model

$$\dot{m}_{ca\,out} = K_{ca\,out}(P_{ca} - P_{rm}) \quad (25)$$

$$\varphi_{O2} = \frac{Inlet\ oxygen\ mass\ flow}{Reacted\ oxygen\ mass\ flow} = \frac{\dot{m}_{O2\,ca\,in}}{\dot{m}_{O2\,rct}} \quad (26)$$

$$\dot{m}_{O2\,rct} = M_{O2} \left(\frac{N_{st} I_{st}}{4F} \right) \quad (27)$$

$$\dot{m}_{O2\,ca\,in} = x_{O2\,ca\,in} * \dot{m}_{a\,ca\,in} \quad (28)$$

$$x_{O2\,ca\,in} = \frac{y_{O2\,ca\,in} M_{O2}}{(y_{O2\,ca\,in} M_{O2}) + (1 - y_{O2\,ca\,in}) M_{N2}} \quad (29)$$

4. Return Manifold Model

$$\dot{m}_{rm\,out} = \frac{C_{D,rm} A_{T,rm} P_{rm}}{\sqrt{R_A T_{rm}}} \left(\frac{P_{atm}}{P_{rm}} \right)^{\frac{1}{\gamma}} \left\{ \frac{2\gamma}{\gamma-1} \left[1 - \left(\frac{P_{atm}}{P_{rm}} \right)^{\frac{\gamma-1}{\gamma}} \right] \right\}^{\frac{1}{2}} \quad (30)$$

If

$$\left(\frac{P_{atm}}{P_{rm}} \right) > \left(\frac{2}{\gamma+1} \right)^{\frac{\gamma}{(\gamma-1)}} \quad (31)$$

Else:

$$\dot{m}_{rm\,out} = \frac{C_{D,rm} A_{T,rm} P_{rm}}{\sqrt{R_A T_{rm}}} (\gamma)^{\frac{1}{2}} \left(\frac{2}{\gamma+1} \right)^{\frac{\gamma+1}{2(\gamma-1)}} \quad (32)$$

5. Cell Electrochemical Model

$$V_{st} = N_{st} * [E_{nerst} - V_{ohm}(\lambda_m) - V_{concentration}(P_{ca}) - V_{act}(\varphi_{O2})] \quad (33)$$

$$E_{nerst} = 1.229 - (0.85 * T_{st} * 10^{-3}) + \left((4.3085 * T_{st} * 10^{-5}) * \left(\log_e(\mathcal{P}_{H2}) + 0.5 * \log_e(\mathcal{P}_{O2}) \right) \right) \quad (34)$$

$$V_{ohm} = j * A_{act} * \left(R_{elec} + \left(\frac{\delta_m}{A_{act} * (0.5139 * \lambda_m - 0.326) * e^{1268\left(\frac{1}{303} - \frac{1}{T_{st}}\right)}} \right) \right) \quad (35)$$

$$V_{concentration} = R_A * \frac{T_{st}}{2F} * \left(1 + \frac{1}{\phi}\right) * \log_e\left(\frac{i_l}{i_l - j}\right) \quad (36)$$

$$V_{act} = R_A * \frac{T_{st}}{2\phi F} * \log_e\left(\frac{j + j_n}{j_{ref} * \alpha_{O2}{}^{\beta}}\right) + a * \varphi_{O2}{}^{b} \quad (37)$$

Nomenclature & Symbols

Symbols Used	Definition	Unit
ω_{cp}	Compressor speed	rad/s
τ_{cm}	Torque produced by the motor	N-m
τ_{cp}	Compressor Load Torque	N-m
J_{cp}	Combined inertia of motor and compressor	kg.m^2
P_{sm}	Supply manifold pressure	bar
R_A	Gas constant	J/(mol.K)
T_{cp}	Temperature at compressor	°C
$\dot{m}_{cp}$	Mass flow out of the compressor	kg/s
$\dot{m}_{sm}$	Mass flow out of supply manifold	kg/s
V_{sm}	Supply manifold volume	m^3
P_{ca}	Cathode pressure	bar
T_{st}	Stack temperature	°C
$\dot{m}_{ca}$	Mass flow at the cathode	kg/s
V_{ca}	Cathode volume	m^3
K_{CaCur}	Calibratable Parameter	bar/s/A
I_{st}	Stack current	A
P_{rm}	Return manifold pressure	bar
T_{rm}	Return manifold temperature	°C
V_{rm}	Return manifold volume	m^3
$\dot{m}_{rm}$	Mass flow into the return manifold	kg/s
λ_m	Membrane water content	-
N_{st}	No of fuel cell in stack	-
A_{act}	Cell effective area	m²
λ_{ca}	Water content cathode side	-
λ_{an}	Water content of anode	-
δ_m	Membrane thickness	m
V_m	Membrane volume	m³
D_w	Diffusion coefficient of water in the membrane	m²/s
V_{st}	Fuel cell stack terminal voltage	V
V_{ohm}	Ohmic voltage	V
V_{act}	Voltage – active cell area	V
φ_{O2}	Oxygen excess ratio	-
η_{cm}	Mechanical efficiency of the motor	-
k_t	Motor parameter	-
R_{cm}	Motor parameter	-
k_v	Motor parameter	-
C_p	Specific heat capacity of air	-

T_{atm}	Ambient temperature	K
η_{cp}	Efficiency of compressor	-
P_{atm}	Atmospheric pressure	bar
γ	Ratio of specific heats	-
K_{sm}	Supply manifold restriction parameter	-
K_{ca}	Cathode restriction parameter	-
$\dot{m}_{O2}$	Mass flow of oxygen into cathode	kg/s
M_{O2}	Oxygen molar mass	kg/mole
F	Faraday constant	-
x_{O2}	Oxygen mass fraction	-
$\dot{m}_a$	Mass flow of air	kg/s
y_{O2}	Molar percentage of oxygen in air	-
M_{N2}	Nitrogen molar mass	kg/mole
C_D	Orifice drag coefficient	-
RH	Relative humidity	-
D_λ	Oxygen diffusivity	m^2/s
$\mathcal{P}_{H2}$	Partial pressure of hydrogen	bar
$\mathcal{P}_{O2}$	Partial pressure of oxygen	bar
R_{elec}	Lumped electrical resistance	ohm
ϕ	Charge transfer coefficient	-
i_n	Internal current density	A/m2
i_{ref}	Reference exchange current density	A/m2
β	Calibratable Parameter	-
a	Calibratable Parameter	-
b	Calibratable Parameter	-
n	Number of states	-
m	Number of inputs	-
N	Prediction Horizon	-
A	A matrix of the continuous system	-
B	B matrix of the continuous system	-
C	C matrix of the continuous system	-
D	D matrix of the continuous system	-
A_d	A matrix of the discrete system	-
B_d	B matrix of the discrete system	-
p_{fs}	Power output of the fuel cell	Watts
$\boldsymbol{u_e}$	Nominal input for linearization	
$\boldsymbol{x_e}$	Nominal states from the linearized model	
y_e	Nominal output from the linearized model	

Works Cited

[1] J. Han, S. Yu, and S. Yi, "Oxygen excess ratio control for proton exchange membrane fuel cell using model reference adaptive control," *Int J Hydrogen Energy*, vol. 44, no. 33, 2019, doi: 10.1016/j.ijhydene.2019.05.041.

[2] M. A. Danzer, J. Wilhelm, H. Aschemann, and E. P. Hofer, "Model-based control of cathode pressure and oxygen excess ratio of a PEM fuel cell system," *J Power Sources*, vol. 176, no. 2, 2008, doi: 10.1016/j.jpowsour.2007.08.049.

[3] A. Mele, P. Dickinson, and M. Mattei, "Nonlinear model predictive control for efficient and robust airpath management in fuel cell vehicles," *Int J Hydrogen Energy*, vol. 48, no. 75, 2023, doi: 10.1016/j.ijhydene.2023.03.398.

[4] J. Chen, Z. Liu, F. Wang, Q. Ouyang, and H. Su, "Optimal oxygen excess ratio control for PEM fuel cells," *IEEE Transactions on Control Systems Technology*, vol. 26, no. 5, 2018, doi: 10.1109/TCST.2017.2723343.

[5] J. T. Pukrushpan, A. G. Stefanopoulou, and H. Peng, *Control of Fuel Cell Power Systems*. London: Springer London, 2004. doi: 10.1007/978-1-4471-3792-4.

[6] C. Hahnel, V. Aul, and J. Horn, "Power efficient operation of a PEM fuel cell system using cathode pressure and excess ratio by nonlinear model predictive control," in *2015 European Control Conference (ECC)*, IEEE, Jul. 2015, pp. 3340–3345. doi: 10.1109/ECC.2015.7331050.

[7] A. G. Haddad, I. Boiko, and A. Al-Durra, "Air-flow control in fuel cells using delay-based load governor and feedforward augmented dynamic inversion," *ISA Trans*, vol. 128, 2022, doi: 10.1016/j.isatra.2021.10.003.

Other References

[1] O. Z. Sharaf and M. F. Orhan, "An overview of fuel cell technology: Fundamentals and applications," *Renewable and Sustainable Energy Reviews*, vol. 32. 2014. doi: 10.1016/j.rser.2014.01.012.

[2] X. Ye, C. Shen, T. Zhang, and Z. Song, "Anode Pressure Control with Fuzzy Compensator in PEMFC System," Apr. 2021. doi: 10.4271/2021-01-0121.

[3] Z. Liu, J. Chen, S. Chen, L. Huang, and Z. Shao, "Modeling and Control of Cathode Air Humidity for PEM Fuel Cell Systems," in *IFAC-PapersOnLine*, 2017. doi: 10.1016/j.ifacol.2017.08.943.

[4] M. A. Danzer, S. J. Wittmann, and E. P. Hofer, "Prevention of fuel cell starvation by model predictive control of pressure, excess ratio, and current," *J Power Sources*, vol. 190, no. 1, 2009, doi: 10.1016/j.jpowsour.2008.12.089.

[5] J. T. Pukrushpan, A. G. Stefanopoulou, and H. Peng, "Control of Fuel Cell Breathing," *IEEE Control Syst*, vol. 24, no. 2, 2004, doi: 10.1109/MCS.2004.1275430.

[6] S. Liu, Y. Bin, Y. Li, and B. Scheppat, "Hierarchical MPC Control Scheme for Fuel Cell Hybrid Electric Vehicles," in *IFAC-PapersOnLine*, 2018. doi: 10.1016/j.ifacol.2018.10.151.

[7] J. Chen, Z. Liu, F. Wang, Q. Ouyang, and H. Su, "Optimal oxygen excess ratio control for PEM fuel cells," *IEEE Transactions on Control Systems Technology*, vol. 26, no. 5, 2018, doi: 10.1109/TCST.2017.2723343.

[8] J. Han, S. Yu, and S. Yi, "Oxygen excess ratio control for proton exchange membrane fuel cell using model reference adaptive control," *Int J Hydrogen Energy*, vol. 44, no. 33, 2019, doi: 10.1016/j.ijhydene.2019.05.041.

[9] J. K. Gruber, C. Bordons, and A. Oliva, "Nonlinear MPC for the airflow in a PEM fuel cell using a Volterra series model," *Control Eng Pract*, vol. 20, no. 2, 2012, doi: 10.1016/j.conengprac.2011.10.014.

[10] E. Bacher-Chong, M. A. Ayubirad, Z. Qiu, H. Wang, A. Goshtasbi, and H. R. Ossareh, "Efficiency-Aware and Constraint-Aware Control of PEMFC Air-Path using a Reference Governor and MIMO Internal Model Controller," in *Proceedings of the American Control Conference*, 2022. doi: 10.23919/ACC53348.2022.9867418.

[11] H. Chen, Z. Liu, X. Ye, L. Yi, S. Xu, and T. Zhang, "Air flow and pressure optimization for air supply in proton exchange membrane fuel cell system," *Energy*, vol. 238, 2022, doi: 10.1016/j.energy.2021.121949.

[12] M. Solsona, C. Kunusch, and C. Ocampo-Martinez, "Control-oriented model of a membrane humidifier for fuel cell applications," *Energy Convers Manag*, vol. 137, 2017, doi: 10.1016/j.enconman.2017.01.036.

[13] K. H. Wong, K. H. Loo, Y. M. Lai, S. C. Tan, and C. K. Tse, "A theoretical study of inlet relative humidity control in PEM fuel cell," *Int J Hydrogen Energy*, vol. 36, no. 18, 2011, doi: 10.1016/j.ijhydene.2011.06.017.

[14] S. Laghrouche, I. Matraji, F. S. Ahmed, S. Jemei, and M. Wack, "Load governor based on constrained extremum seeking for PEM fuel cell oxygen starvation and compressor surge protection," *Int J Hydrogen Energy*, vol. 38, no. 33, 2013, doi: 10.1016/j.ijhydene.2013.08.109.

[15] C. Bao, M. Ouyang, and B. Yi, "Modeling and control of air stream and hydrogen flow with recirculation in a PEM fuel cell system-I. Control-oriented modeling," *Int J Hydrogen Energy*, vol. 31, no. 13, 2006, doi: 10.1016/j.ijhydene.2006.02.031.

[16] A. Mele, P. Dickinson, and M. Mattei, "Nonlinear model predictive control for efficient and robust airpath management in fuel cell vehicles," *Int J Hydrogen Energy*, vol. 48, no. 75, 2023, doi: 10.1016/j.ijhydene.2023.03.398.

[17] J. T. Pukrushpan, A. G. Stefanopoulou, and H. Peng, *Control of Fuel Cell Power Systems*. London: Springer London, 2004. doi: 10.1007/978-1-4471-3792-4.

[18] J. Chen, Z. Liu, F. Wang, Q. Ouyang, and H. Su, "Optimal oxygen excess ratio control for PEM fuel cells," *IEEE Transactions on Control Systems Technology*, vol. 26, no. 5, 2018, doi: 10.1109/TCST.2017.2723343.

[19] J. T. Pukrushpan, A. G. Stefanopoulou, and H. Peng, *Control of Fuel Cell Power Systems*. London: Springer London, 2004. doi: 10.1007/978-1-4471-3792-4.